On reconstruction and time reversal in thermoacoustic tomography in acoustically homogeneous and inhomogeneous media

Yulia Hristova, Peter Kuchment, and Linh Nguyen

Mathematics Department, Texas A& M University, College Station, TX 77845, USA

E-mail: ygh@math.tamu.edu, kuchment@math.tamu.edu, lnguyen@math.tamu.edu

Abstract. The paper starts with a comparative discussion of features and limitations of the three types of recent approaches to the reconstruction in thermoacoustic/photoacoustic tomography: backprojection formulas, eigenfunction expansions, and time reversal. The latter method happens to be the least restrictive. It is then considered in more detail, e.g. its relation to trapping properties of the medium. The time reversal method is exact only in the case of a constant sound speed in odd dimension, due to validity of the Huygens' principle. The next best case is of non-trapping speed in odd dimensions. The authors provide $2D$ examples and discuss the features of numerical reconstructions for constant and variable (both non-trapping and trapping) speeds, showing that this technique works surprisingly well even under the most unfavorable circumstances (variable, and even trapping sound speed in $2D$). In particular, a "limited view" effect due to trapping is observed and explained. Finally, an initial consideration of the problem of sound speed recovery is also provided.
Keywords: Tomography, thermoacoustic, wave equation.

AMS classification scheme numbers: 35L05, 92C55, 65R32, 44A12

Submitted to: *Inverse Problems*

1. Introduction

The description of the set-up of thermoacoustic tomography, which we will dub TAT, can be found in several recent books and survey papers, e.g. in [2, 17, 30, 34, 48–50, 53, 61, 62, 64]. We thus provide here a very brief sketch only.

A short electromagnetic (EM) pulse is sent through the biological object of interest. Some part of the EM energy is absorbed throughout the object. Knowing the distribution function $a(x)$ of the absorption would provide an invaluable diagnostic tool, since cancerous cells absorb several times more energy in these ranges than the healthy ones (e.g., [31, 48, 49, 61, 64]). Thus, finding function $a(x)$ is a major goal. An interesting mechanism is used to image a. Namely, absorbed energy causes thermoelastic expansion of the tissue, which in turn leads to a pressure (ultrasound) wave $p(x, t)$

propagating through the object. This pressure is measured by transducers distributed over an **observation surface** S surrounding the object. (The most common geometry is when S is a sphere. Cylinders, planes, and cubes have also been studied as observation surfaces.) The value $f(x) = p(x, 0)$ of the pressure at the initial moment of time $t = 0$, i.e. at the moment of irradiation, is not exactly the energy absorption function $a(x)$, but rather is roughly proportional to it (the reader can find the details in [48, 49, 61, 64]). One thus concentrates on the recovery of $f(x)$. Ultrasound imaging has rather low contrast, but in TAT the contrast comes from the one in electromagnetic absorption, while ultrasound provides its high resolution.

The commonly accepted mathematical model of TAT looks as follows [11, 57]:

$$\begin{cases} p_{tt} = c^2(x)\Delta_x p, & t \geq 0, \quad x \in \mathbb{R}^3 \\ p(x, 0) = f(x), & p_t(x, 0) = 0, \\ p(y, t) = g(y, t) & \text{for } y \in S, \quad t \geq 0. \end{cases} \tag{1}$$

Here $c(x)$ is the speed of the ultrasound propagation in the tissue, $g(y, t)$ is the measured data, i.e. the value of the pressure at the time t measured at the transducer's location $y \in S$, p_t, p_{tt} denote the first and second time derivatives, and Δ_x is the Laplace operator with respect to the spatial variable x.

The main problem now can be formulated as follows: given the sound speed $c(x)$ and measured data $g(y, t)$ in (1), find the initial value $f(x)$ of the pressure $p(x, t)$. This initial value is the TAT image.

A $2D$ version of this problem is also important, since it arises when line, rather than point detectors are used [6, 7, 23–25, 51, 52].

There is also an issue concerning knowledge of the sound speed, which is usually assumed to be constant, or is measured by a prior transmission ultrasound scan [28]. A not well studied problem is of recovery of both the sound speed and the image from the measured data g. We address it briefly in Section 5, but in the rest of the paper we will assume the sound speed to be known.

While in thermoacoustic tomography electromagnetic waves of radio frequency range are used to trigger the ultrasound signal, in the so called photo- (or opto-) acoustic tomography (PAT) [31, 48, 49, 61, 62], the frequency lies in the visual or near infra-red ranges. For the mathematical purpose of this paper, there is no distinction between these methods, so we will refer to TAT only, while the results apply to PAT as well.

2. Discussion of various inversion methods

A first attempt to look at the problem of recovery f from g in (1) might lead to a brief confusion (which turns out to be fruitful): it seems that recovery of the initial data for the wave equation inside the cylinder $C := S \times [0, \infty)$ from the boundary data g is absolutely impossible. Indeed, standard partial differential equation (PDE) theorems (e.g., [14]) claim that imposing **arbitrary** function f as the initial data, one can find a solution in the cylinder such that the boundary data g are satisfied. In other words, f

can be any function, and thus data g carries no information about f at all, which means that TAT is plainly impossible. So, what is wrong with this consideration? The answer is that we have some additional information about the initial data f and the solution p, which makes the problem solvable. Firstly, the function f (essentially our initial energy absorption distribution) has a **bounded support** (usually inside the object being irradiated). Secondly, the wave equation in (1) holds **in the whole space** $\mathbb{R}^3$, rather than inside the cylinder only. These two pieces of information make the crucial difference, since they make the TAT problem solvable and also enable one to understand better the peculiarities of different reconstruction methods.

Let us single out various assumptions that one may or may not use deriving inversion formulas and algorithms for TAT. As we will show later, different known methods in fact use different assumptions, which influences their features and applicability.

2.1. Assumptions used in reconstruction methods for TAT

As it is mentioned in the beginning of Section 2, some *a priori* conditions must be used, otherwise the data g is insufficient for the recovery of the object f. All reconstruction methods in TAT known to the authors use one or more from the following list of conditions:

- The function $f(x)$ to be reconstructed (source) is usually assumed to be supported inside the observation surface. In other words, there are no ultrasound sources outside S. A weaker assumption is that f has a bounded support, but not necessarily confined by S. Even weaker assumption would allow f to have an "infinitely long tail", if only it decays sufficiently fast.
- A method may or may not use the condition that the solution $p(x,t)$ exists in the whole space $\mathbb{R}^3$.
- A reconstruction formula or algorithm might use, instead of assumptions on the support of f and validity of the wave equation in the whole space, the weaker condition that the solution decays inside S (in some cases a qualified rate of decay is needed). This condition is weaker, since for the wave equation in the whole space and a compactly supported initial perturbation, normally the solution decays with time inside any bounded domain, in particular inside the observation surface S (see more detailed discussion of this later on in this text).
- A method may or may not use the information that the initial time derivative $p_t(x,t)$ vanishes at $t=0$ (although this condition is normally satisfied in TAT).
- Inversion might work for an arbitrary observation surface S, or just for a specific one (usually a sphere).
- Finally, inversion method might work for the constant sound speed only, or for variable speeds under some conditions (non-trapping, as we will see, is an important example), or for rather general sound speeds.

As we will see, the choice of the assumptions from this list that are incorporated into a method influences its features and applicability significantly.

2.2. Discussion of main inversion methods in terms of their assumptions and related features

After the recent progress in reconstruction methods for TAT, one currently has a choice between three main types of reconstruction procedures for closed observation surfaces (not counting algebraic methods):

Filtered backprojection formulas. Till the paper [17] appeared a few years ago, it had not been clear whether closed form backprojection type formulas could be written for any closed observation surface S. In [17], a variety of such formulas was obtained in odd dimensions under the assumption of constant sound speed (one can assume that $c(x) = 1$) and S being a sphere of radius R. In $3D$, three such formulas read

$$\begin{aligned} f(x) &= -\tfrac{1}{8\pi^2 R}\Delta_x \int\limits_S g(y, |y-x|)dA(y), \\ f(x) &= -\tfrac{1}{8\pi^2 R}\int\limits_S \left(\tfrac{d^2}{dt^2} g(y,t)\right)\Big|_{t=|y-x|} dA(y), \\ f(x) &= -\tfrac{1}{8\pi^2 R}\int\limits_S \left(\tfrac{d}{dt}\left(\tfrac{1}{t}\tfrac{d}{dt}\tfrac{g(y,t)}{t}\right)\right)\Big|_{t=|y-x|} dA(y). \end{aligned} \tag{2}$$

These formulas were also extended later to even dimensions in [16]. A different set of formulas was obtained in all dimensions in [36] (in $3D$, the formula of [36] was obtained earlier in [63]). One can find a detailed discussion and comparison of these formulas in [2, 34].

These series of inversion formulas have been tested numerically and all perform well.

Eigenfunction expansion method. Long time before the first backprojection type formula was discovered, series expansions had been available for the case of a constant sound speed and transducers placed along a sphere S surrounding the object [45, 46]. In these formulas, rotational invariance of the problem was exploited, which allowed one to expand into Fourier series with respect to the polar angle. This approach was extended to the constant speed and arbitrary closed observation surface and modified by the usage of the eigenfunctions of the Laplacian with Dirichlet conditions on S in [37] (see also the circular case in [25]). This was carried over to variable sound speed and arbitrary closed observation surface in [1]. The results of [1, 37] can be viewed as specific instances of the following statement:

Theorem 1. *[1] Let B be the domain bounded by S. Function $f(x)$ can be reconstructed inside B from the data g as the following $L^2(B)$-convergent series:*

$$f(x) = \sum_k f_k \psi_k(x), \tag{3}$$

where $\psi_k(x), \lambda_k^2$ are the eigenfunctions and eigenvalues of the operator $-c^2(x)\Delta$ in B with zero Dirichlet conditions on S. The Fourier coefficients f_k can be recovered using one of the following formulas:

$$f_k = \lambda_k^{-2} g_k(0) - \lambda_k^{-3} \int_0^\infty \sin(\lambda_k t) g_k''(t) dt,$$
$$f_k = \lambda_k^{-2} g_k(0) + \lambda_k^{-2} \int_0^\infty \cos(\lambda_k t) g_k'(t) dt, \ \ or \tag{4}$$
$$f_k = -\lambda_k^{-1} \int_0^\infty \sin(\lambda_k t) g_k(t) dt = -\lambda_k^{-1} \int_0^\infty \int_S \sin(\lambda_k t) g(x,t) \overline{\frac{\partial \psi_k}{\partial \nu}(x)} dx dt.$$

Here

$$g_k(t) = \int_S g(x,t) \overline{\frac{\partial \psi_k}{\partial \nu}(x)} dx$$

and ν denotes the external normal to S.

It was shown in [37] that using this formula for the case of S being a cube and a constant sound speed leads to extremely fast and precise reconstructions. It is not clear whether the formulas (3)-(4) for the variable speed can be effectively implemented.

Time reversal method. This technique was probably explicitly suggested for the first time in [17] for odd dimensions and constant sound speed and since then tried successfully in a few cases, e.g. in [8, 20, 21]. The idea is very simple: if the sound speed is constant and the spatial dimension is odd, the Huygens' principle holds (e.g., [10]), which states that for any initial source with a bounded support, the wave leaves any bounded domain in a finite time. In other words, under the stated conditions, there is a moment T (the longest time it takes the wave to traverse the domain B), such that the solution $p(x,t)$ of (1) vanishes inside B for any $t > T$. Then one can impose zero initial conditions at $t = T$ and boundary conditions equal to the measured data g and solve (1) in the reversed time direction, thus arriving at $t = 0$ to the function $f(x)$.

When the dimension is even, or when the sound speed is not constant, the Huygens' principle does not hold anymore (Huygens' principle holds rarely, and there is a large body of research devoted to it, see [22] and references therein). However, there is still some decay of solutions in bounded domain, for which estimates can be provided if the sound speed is **non-trapping** (see details in Section 3). Thus, time reversal method should somehow work for sufficiently large cut-of time T. We discuss this issue in Section 4

Let us now describe what assumptions are used in each of these approaches, and thus what are their limitations.

Assumptions of filtered backprojection formulas. All known formulas of the filtered backprojection type assume constant sound speed and thus are not available for acoustically inhomogeneous media. The only closed bounded surface S for which

such formulas are known is a sphere. It is also assumed that the wave equation holds in the whole space. However, even for S being a sphere and the sound speed constant, a significant additional assumption is that the object f to be recovered is confined inside the observation surface S (i.e., no signal is coming from outside of S). It is known (see [2, 34]) that if f has some part of its support reaching outside S, all known formulas of backprojection type reconstruct f incorrectly **inside** S. Moreover, different backprojection formulas lead to different (incorrect) reconstructions. Apparently no backprojection type formula without this deficiency is known at this time, and it is not clear whether such a formula can exist (see [2, 34] for a discussion). Thus, although backprojection type formulas, when available and when assumptions are satisfied, lead to high quality reconstructions, their applicability is limited by the assumptions of S being a sphere, speed being constant, and absence of sources outside of S.

Assumptions of the eigenfunction expansion method. The eigenfunction expansion approach theoretically works for any closed surface and for variable sound speeds. The only significant assumption for the method to work is that the solution decays sufficiently fast inside S, which holds, for instance, if the initial source f has bounded support (not necessarily contained inside S) and the sound speed satisfies a non-trapping condition [1]. This makes the method seemingly very attractive, and it has been shown to be extremely efficient for constant sound speed and S being a cube [37]. However, it is not without its own pitfalls. Indeed, although it works theoretically for variable (non-trapping) sound speed, it is not clear at all whether it can be efficiently implemented numerically in this case.

Assumptions of the time reversal method. The time reversal method works for arbitrary geometry of the closed observation surface S. The sound speed can be variable. The source f does not have to be supported inside S. In fact, the only important condition is that the solution inside S decays with time. This happens even for "bad" trapping speeds, although the decay can be slow, and thus a larger cut-of time T might be needed. In the case of a non-trapping speed, the decay is known to be sufficiently fast (e.g., exponential in odd dimensions), see Section 3. It is not required that the initial time derivative of the pressure is equal to zero. Finally, the method can be easily implemented for acoustically inhomogeneous media and arbitrary closed observation surfaces using simple numerical schemes for the wave equation.

This discussion shows that the least sensitive to any restrictions and the most versatile among these methods is the time reversal one. We thus devote the next two sections for its discussion and testing.

3. Local energy decay and non-trapping conditions

As mentioned above, the time reversal method is based upon only one condition - decay of the solution in the domain B bounded by the observation surface S. Therefore, we address here the known results on such decay, which have a rather long history (e.g., [9, 12, 38, 40, 41, 55, 58, 59] and references therein). We will provide only a brief summary of the local (i.e., in a bounded domain) decay results and the relevant references.

Consider the wave equation problem in $\mathbb{R}^n$, $n \geq 2$:

$$\begin{cases} p_{tt} = c^2(x)\Delta_x p, \quad t \geq 0, \quad x \in \mathbb{R}^n \\ p(x,0) = f_1(x), \quad p_t(x,0) = f_2(x), \end{cases} \tag{5}$$

where we will assume the initial data functions f_1, f_2, and the sound speed $c(x)$ to be sufficiently smooth (in the discussion of the trapping below they are assumed to be infinitely differentiable). The functions f_j are assumed to be compactly supported, and the sound speed is assumed to stabilize to 1 at large distances, i.e. $c(x) - 1$ is compactly supported.

Let also B be a bounded domain (in the thermoacoustic application, it is the interior of the observation surface S). We are interested in the decay of the solution $p(x,t)$ inside B when $t \to \infty$. In the best of situations, when the dimension n is odd and the sound speed is constant, Huygens' principle [10, 22] says that after a finite time the solution will vanish identically in B. No such luck, though, in even dimensions and/or when the sound speed is variable. So, let us summarize what is known in this regard. In order to describe the energy decay results, we need to introduce a non-trapping condition on $c(x)$. Consider the following Hamiltonian system in the space $\mathbb{R}^{2n}_{x,\xi}$ of pairs (x,ξ) of n-dimensional vectors, with the Hamiltonian $H = \frac{c^2(x)}{2}|\xi|^2$:

$$\begin{cases} x_t' = \frac{\partial H}{\partial \xi} = c^2(x)\xi \\ \xi_t' = -\frac{\partial H}{\partial x} = -\frac{1}{2}\nabla\left(c^2(x)\right)|\xi|^2 \\ x|_{t=0} = x_0, \xi|_{t=0} = \xi_0. \end{cases} \tag{6}$$

The solutions of this system are called **bicharacteristics** and their projections into $\mathbb{R}^n_x$ are **rays**.

Definition 2. *We will say that the* **non-trapping condition** *holds, if all rays (with $\xi_0 \neq 0$) tend to infinity when $t \to \infty$.*

A simple example of a trapping velocity $c(x)$ is the one where in an annulus $A = \{x \,|\, r_1 < |x| < r_2\}$ one has $c(x) = |x|$ (behavior of $c(x)$ outside A is irrelevant). It is easy to check then that the projection of a bicharacteristic starting at a point (x_0, ξ_0) such that $x_0 \in A$ and $\xi_0 \perp x_0$ is the circle $|x| = |x_0|$, which is thus a trapped ray. We will use such trapping velocities in some examples later on in this text.

Since it is known that singularities of solutions propagate along bicharacteristics [27, 58], non-trapping implies that with time, the solution becomes smooth in any finite domain B, even if the initial data were not smooth. Moreover, it has been discovered that non-trapping also implies certain decay of the solution in any compact domain (trapping

slows down decay immensely, although does not stop it completely). This local (i.e., in a compact domain B, as in TAT) decay of solutions with compactly supported initial data also depends on the spatial dimension (odd dimensions are better). We summarize below some known results concerning this decay (e.g., [12, 38, 40, 58, 59] and references therein).

Non-trapping speed.

Theorem 3. *([58, 59], see also [12] for a brief description of this result.)*
If the non-trapping condition is satisfied, then for any multi-index $\alpha = (\alpha_0, \alpha_1, ...\alpha_n)$*, the following estimate holds for the solution of (5):*

$$\left| \frac{\partial^{|\alpha|}}{\partial_t^{\alpha_0} \partial_{x_1}^{\alpha_1} ... \partial_{x_n}^{\alpha_n}} \right| \leq C\eta(t) \left(\|f_1\|_{L_2} + \|f_2\|_{L_2} \right), x \in B, \tag{7}$$

where the function $\eta(t)$ *that characterizes the decay is* $t^{-n-\alpha_0+1}$ *when the dimension* n *is even and* $e^{-\epsilon t}$ *for some* $\epsilon > 0$ *when* n *is odd.*
This result shows that in the non-trapping case, the rate of the local decay of solutions is exponential in odd dimensions and only power in even dimensions, and it worsens when the even dimension gets smaller. Thus, if the sound speed is non-trapping, the slowest decay occurs in dimension two.

Trapping speed. Even in the trapping case, the local energy

$$\frac{1}{2} \int_B \left(|p_x|^2 + c^{-2}(x)|p_t|^2| \right) dx$$

of the solution p in any compact domain B decays to zero [38, 40]. However, there is no general function $\eta(t)$ as in the Theorem above, which would give the rate of this decay in terms of the initial energy [55]. There are such estimates in terms of an appropriate norm of the initial data, but the decay is only logarithmic [9].

We see that the worst case scenario for the decay of solutions is the two dimensional case, especially when trapping occurs.

4. Time reversal - a discussion and numerical results

We have already briefly described the time reversal method. Namely, the solution $p(x, t)$ of (1) decays with time inside the observation surface. One can thus try to choose a sufficiently large time T such that one can assume approximately that at that time the pressure p and its time derivative p_t vanish. Using this zero initial condition for $t = T$ and the measured TAT data $g(y, t)$ as the boundary data (appropriately phased out to zero near $t = T$), one solves numerically the wave equation back in time and arrives at $t = 0$ to the sought for function $f(x)$. This simple idea can be supported by estimates that show that the error of such reconstruction is small in an appropriate norm. We plan to provide these estimates elsewhere. It is clear that the rate of the decay that one can guarantee influences the choice of the appropriate T and thus the quality of the

reconstruction. Our discussion in the previous section showed that the decay is fastest (exponential) in odd dimensions and under the non-trapping condition on the sound speed. In even dimensions (and still with non-trapping), the decay gets faster with the growth of the dimension. We thus will test the method under the least favorable conditions: in $2D$ and with variable speeds, including those that are trapping.

In the computations below we used the most simpleminded implementation of finite difference approximations for the wave equation in order to create the data $g(y,t)$ and then a similar simpleminded time reversal solution. The $2D$ numerical implementation was similar to the finite difference scheme used in [8]. We used Matlab to implement the Rectilinear Finite Difference scheme on a square space grid. For both simulation of the phantom data and reconstruction procedures the boundary of the unit circle S was approximated by the set of interior grid points closest to S. For the simulation of phantom data we solved

$$\begin{cases} p_{tt} - c^2 \triangle p = 0 \qquad \text{in } D \times (0, T_0] \\ p(x,0) = f(x)\ p_t(x,0) = 0 \\ p|_{\partial D} = 0, \end{cases}$$

where $D = [-a,a]^2$ was a square large enough to ensure that no reflections off its boundary could reach S by time T_0. The values of the solution at the approximated S were recorded for all time steps. The time T_0, the square domain D, and the space and time steps sizes were adjusted depending on the simulation. For instance, when using a trapping sound speed, one needs larger times T_0 (and thus, bigger D) to make sure that the solution inside the unit circle has sufficiently decreased before one can cut it off to zero. For the reconstruction part, a similar difference scheme (but a different mesh) was used, this time on the square $[-1.2, 1.2]^2$.

In both forward simulation and reconstruction, the spatial step-size h varied between 0.005 and 0.01, which corresponds to using several hundreds of detectors on the boundary of the unit circle (with a smaller numbers of detectors interpolation would have to be needed). The time step was chosen accordingly, in order to satisfy the stability condition of the finite difference method.

To avoid the inverse crime being committed, two precautions were implemented. First of all, we made sure that different discretizations were used for the forward and inverse computations. Secondly, for several phantoms the computations were repeated using for the forward model a finite element method (the standard implementation of Matlab), while the inverse problem was solved still with finite differences.

4.1. Constant speed

We start with the most favorable situation: a constant speed that we choose to be equal to 1. In this and the other sub-sections, the observation surface is chosen to be the unit circle S on the plane. Thus, it takes time $t = 2$ for the front of the wave moving with the unit speed to cross the disk S.

The numerical phantom consisting of two round objects is shown in Fig. 1. Although the sound speed is constant, there is no Huygens' principle in $2D$, so the

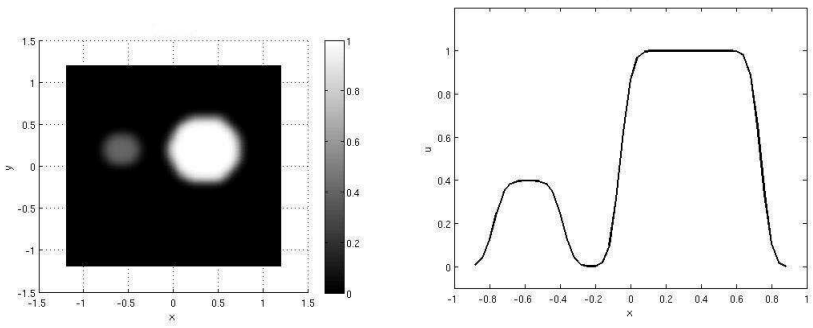

Figure 1. The phantom and its axial profile.

wave is still there at the time $T = 2$ (and in fact, for all times). We try first $T = 2$ and thus use the time reversal enforcing zero conditions at $t = 2$. This leads to the reconstruction shown in Fig. 2. Waiting longer improves the result somewhat (as it

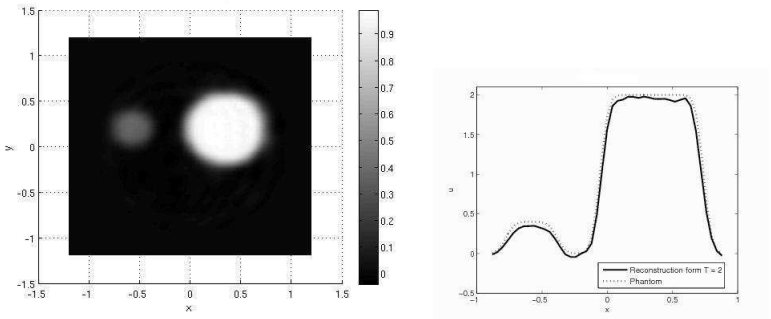

Figure 2. Reconstruction for $c = 1$ and $T = 2$

should), see Fig. 3.

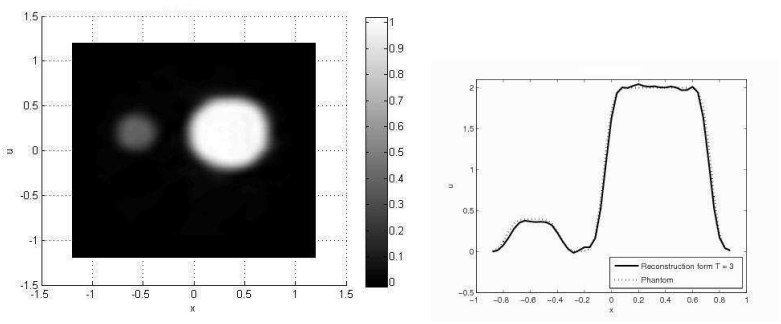

Figure 3. Reconstruction for $c = 1$ and $T = 3$

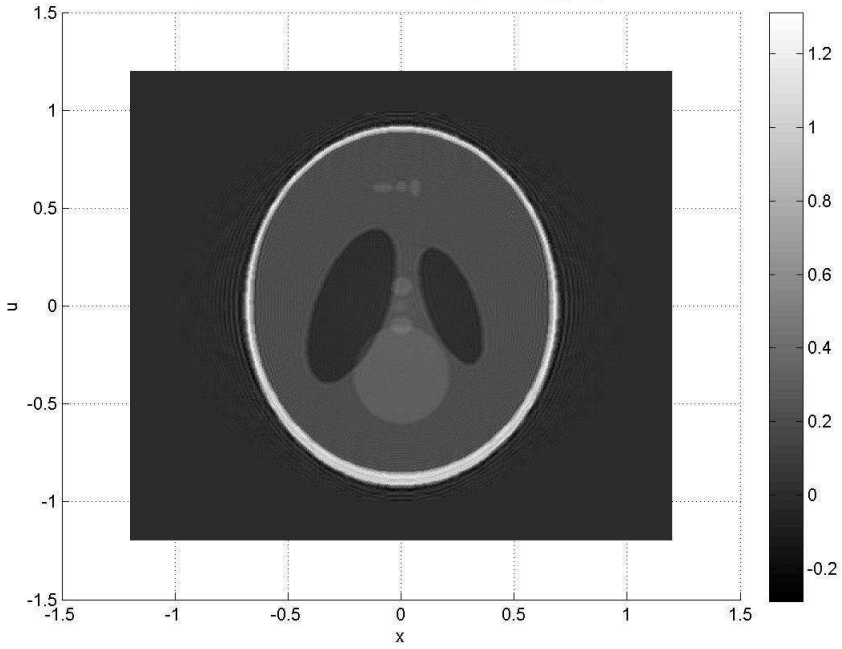

Figure 4. Reconstruction for $c = 1$ and $T = 3$ of the Shepp-Logan phantom

In Fig. 4 one finds a reconstruction of the Shepp-Logan phantom.

These examples show that the time reversal method works rather well with a constant sound speed in $2D$, in spite of it being theoretically not exact (the claim made in [20] that the method is theoretically exact holds only for a constant speed in odd dimensions).

Let us now illustrate some features of time reversal discussed before that are not available with the known backprojection formulas.

First of all, presence of a part of the function $f(x)$ outside the observation surface S does not hinder the reconstruction of f **inside** S. Fig. 5 shows a phantom that has a part of it outside the unit circle S and its reconstruction inside S. Clearly, there are no artifacts, which one would get with the analytic inversion formulas [2, 34].

Another interesting feature is that the initial velocity being zero (which is assumed in all analytic inversion formulas) is not necessary. We will show a corresponding example in the next section, with a variable sound speed. It works even better with a constant speed.

4.2. Non-trapping variable speed

Let us now experiment with the time reversal method for a (known) variable speed under the non-trapping condition.

In Fig. 6 one can see the speed profile and the phantom that were used in calculations, and Fig. 7 shows the corresponding reconstructions.

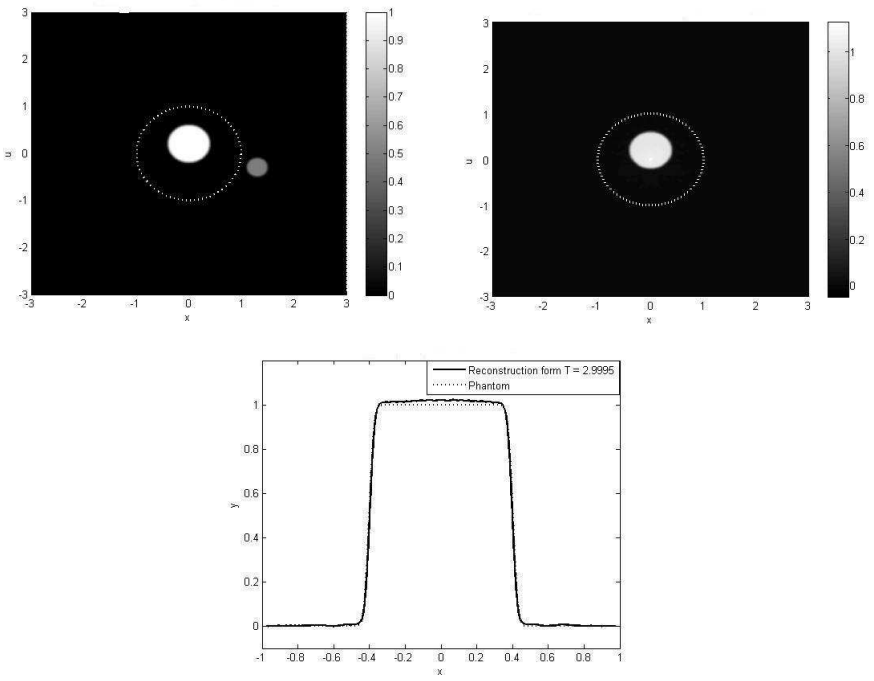

Figure 5. Phantom (left) with a part outside the observation surface, its reconstruction (right), and comparison with the original (bottom).

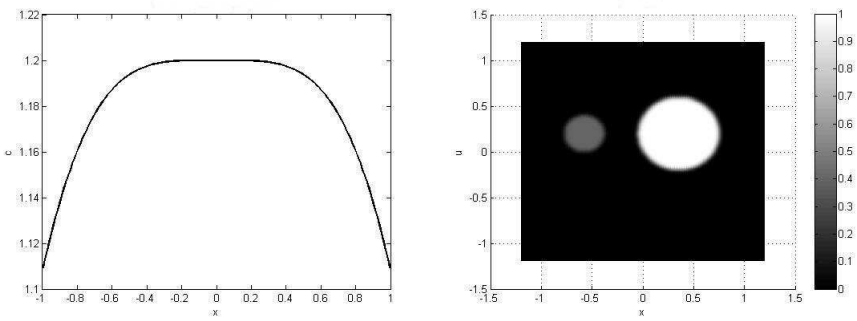

Figure 6. A non-trapping (radial) speed profile (left) and a phantom (right).

We now present an example where the initial velocity is non-zero. Fig. 8 shows the sound speed, the initial value phantom (i.e., $f(x)$ to be reconstructed), and the initial velocity.

The reconstruction of the phantom shown in Fig. 9 confirms that the presence of a non-zero initial velocity does not hamper the reconstruction. Moreover, although this is not of interest for TAT, the initial velocity can also be reconstructed by the time reversal, although it is (expectably) somewhat less stable.

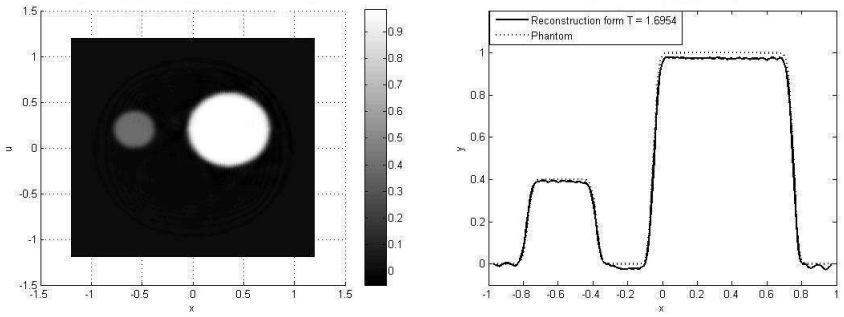

Figure 7. Reconstruction with the non-trapping speed.

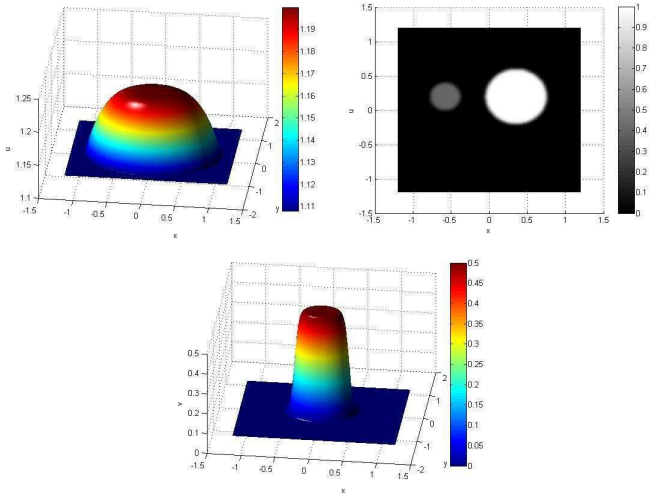

Figure 8. The sound speed, density plot of the initial phantom, and the initial velocity.

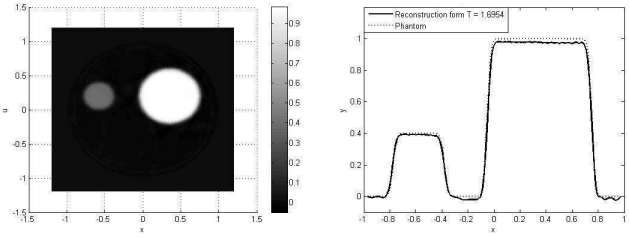

Figure 9. Reconstruction of the phantom in presence of the non-zero initial velocity.

4.3. Trapping variable speed

Let us turn now to the worst case scenario: trapping speeds in $2D$. The simplest way to create a trapping speed, as we have already mentioned, is to use a speed with a "crater profile," which is constant in a small disk, then increases linearly with the radius in an annulus, and then becomes constant again, see Fig. 10

Fig. 11 represents the phantom (its density and surface plots).

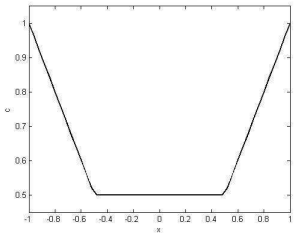

Figure 10. A "crater" trapping speed.

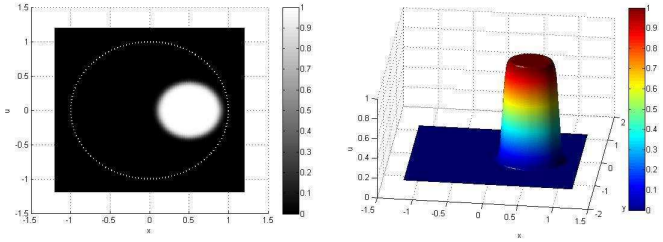

Figure 11. The phantom used for reconstruction with the "crater" sound speed.

Reconstructions for $T = 4, 10,$ and 15 (it takes $t = 3.3863$ for the wave to go across the unit circle) are shown in Fig. 12. One clearly sees that although it takes a longer time, one still eventually reconstructs the phantom. There is, however, a phenomenon that can deteriorate the reconstructions in the trapping situations, and which one should be aware of. We discuss it in the next sub-section.

4.4. Limited view effects due to a trapping speed

Let us use again the same "crater" trapping speed (Fig. 10) and look at the quarter-annulus phantom sitting inside the trapping area and its reconstruction shown in Fig. 13.

These reconstructions appear to show blurring of the radial sides of the phantom, a phenomenon common to incomplete data problems [2, 33, 34, 39, 54, 66, 67]. However, it seems that we collect the data from the whole closed surface S and thus appear to have as complete data as possible. So, what is going on here? Notice that only the radial sides are blurred. It is known that the wavefront set of such a piece-wise smooth phantom consist of points (x, ξ), where x belongs to an interface, and ξ is a normal vector to the interface at this point. In particular, at the radial sides of our phantom, the vector ξ is normal to the radius of S. We have already mentioned the well known fact from the theory of PDEs (see, e.g. [12, 27]) that the singularities propagate along the bicharacteristics. In the case of our crater speed, however, the ray (the x-projection of a bicharacteristic) starting at the radial interface being normal to the radius, is circular and thus never reaches S. This means, that the singularity of the radial interface never shows up as a singularity in the measured data g. It has been

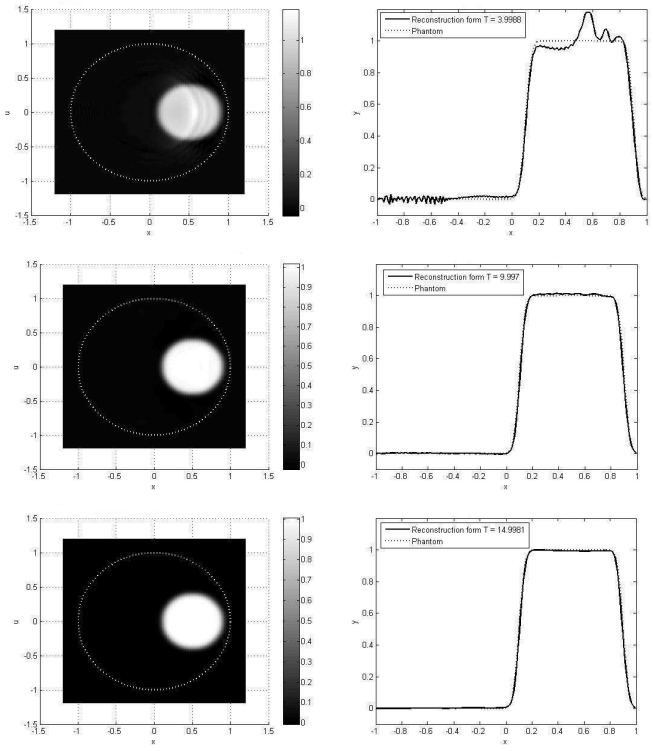

Figure 12. The reconstructions for $T = 4, 10$, and 15 with the "crater" trapping speed.

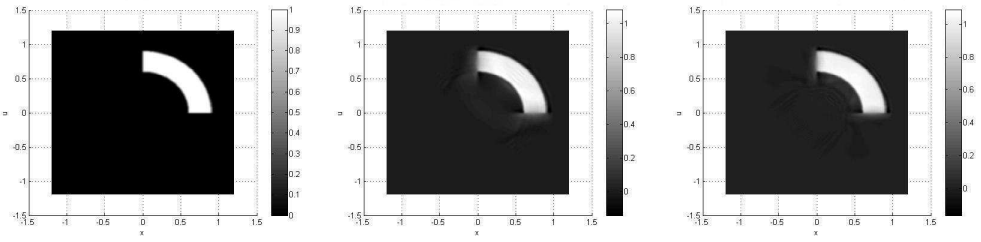

Figure 13. A phantom and its reconstructions for $T = 4$ and 6 with the "crater" trapping speed.

argued then [2, 33, 34, 39, 54, 66, 67] that this piece of the interface cannot be stably reconstructed and thus gets blurred, no matter what reconstruction method is used. Since the rays that start being normal to other parts of the phantom's boundary are not trapped, these parts are reconstructed stably.

Since the blurring might be seen as very slight, we provide more examples to show its presence exactly where one would expect it.

Fig. 14 contains a phantom (and its reconstruction) that is similar to the one in Fig. 13, except that its radial width is larger and thus some part of the phantom reaches into the non-trapping region. The reconstructions confirm the result of our previous discussion: only parts of the boundaries whose normals produce trapped rays

are blurred.

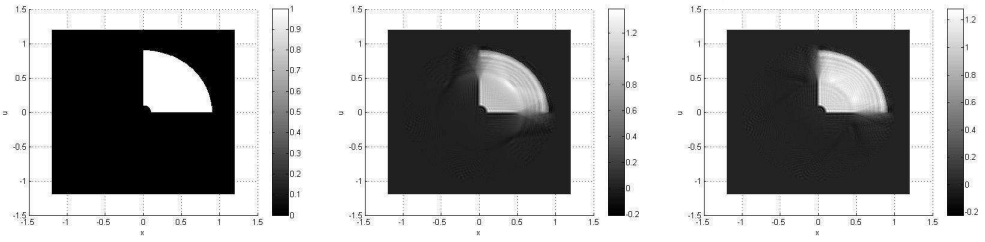

Figure 14. A phantom and its reconstructions for $T = 4$ and 6 with the "crater" trapping speed. The parts of the boundaries not in trapping ring are not blurred.

The reader should notice that if the phantom's boundaries inside the trapping ring were not radial, they would reconstruct sharply, since the related rays would reach S. This is confirmed for instance with the phantom and its reconstruction shown in Fig. 15.

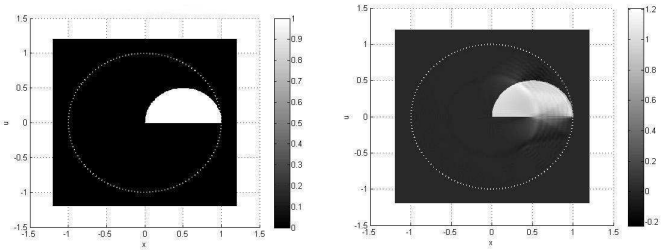

Figure 15. A semi-circular phantom and its reconstructions for $T = 4$ with the "crater" trapping speed. The parts of the boundaries that are in the trapping ring, but such that the normal vectors produce non-trapped rays, are not blurred.

It is interesting to notice what happens with a smaller semi-circular phantom shown in Fig. 16. Here one notices a deterioration near the point on the semi-circular part, where the boundary is tangential to the radius. The reason is that the corresponding ray is trapped. In the reconstruction shown in Fig. 15, this effect did not appear, since the corresponding point was not in the trapping region and thus the relevant ray was escaping.

4.5. Reconstruction with an incorrect speed

In the above discussions, we have always assumed that the sound speed was known, while it is often not. To overcome this, one either tries to recover somehow the speed (e.g., using transmission ultrasound tomography [28, 29]), or assumes some (usually constant) speed. As it has been noted in previous studies (e.g., [28, 29, 65]), it is easy to conclude that using an incorrect sound speed deteriorates both the amplitudes, as

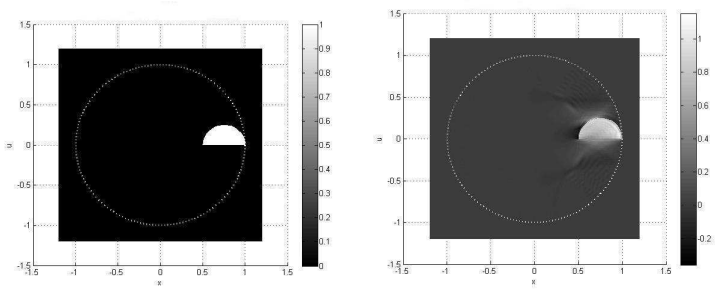

Figure 16. A smaller semi-circular phantom and its reconstructions for $T = 4$ with the "crater" trapping speed. There is a noticeable blurring on the circular boundary at the point where the normal ray is trapped (i.e., where the circle is tangential to the radius).

well as locations of features (e.g., of interfaces) of the image. The example shown below is provided to confirm this. In Fig. 17 one sees the speed map, the phantom, and the overlap of the two. The next Fig. 18 shows the reconstruction for $T = 2.5$ with the true speed used and for $T = 5$ with the average speed. One can easily see both types of deterioration mentioned before. This example also shows the viability of the time reversal in the case of more realistic sound speeds than used before (several different "tissues" are present).

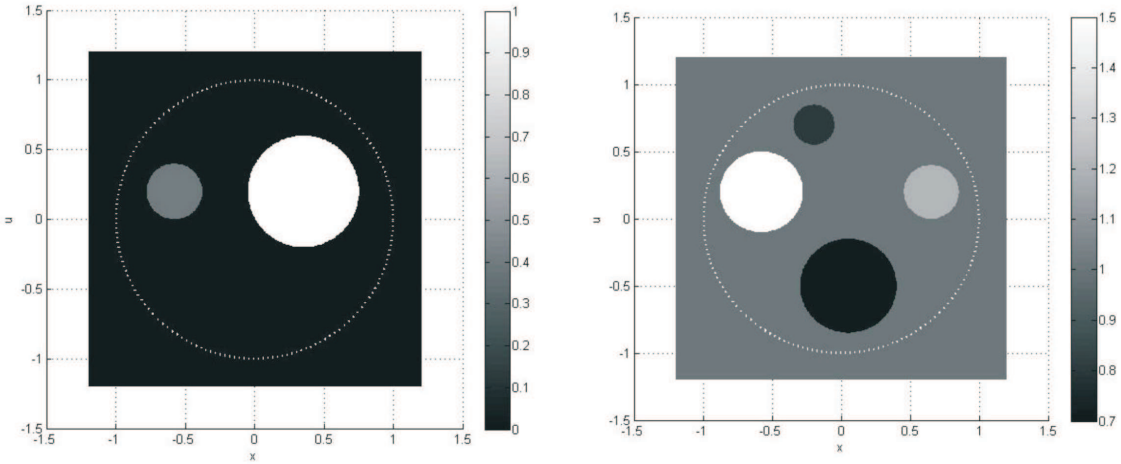

Figure 17. The phantom, the sound speed density plot, and the overlap of the two.

5. Variable speed recovery

Here we briefly address the question of the reconstruction of the sound speed from the TAT data. One of the tested approaches [28, 29] is to use transmission ultrasound tomographic measurement to recover the speed map, which can then be applied for

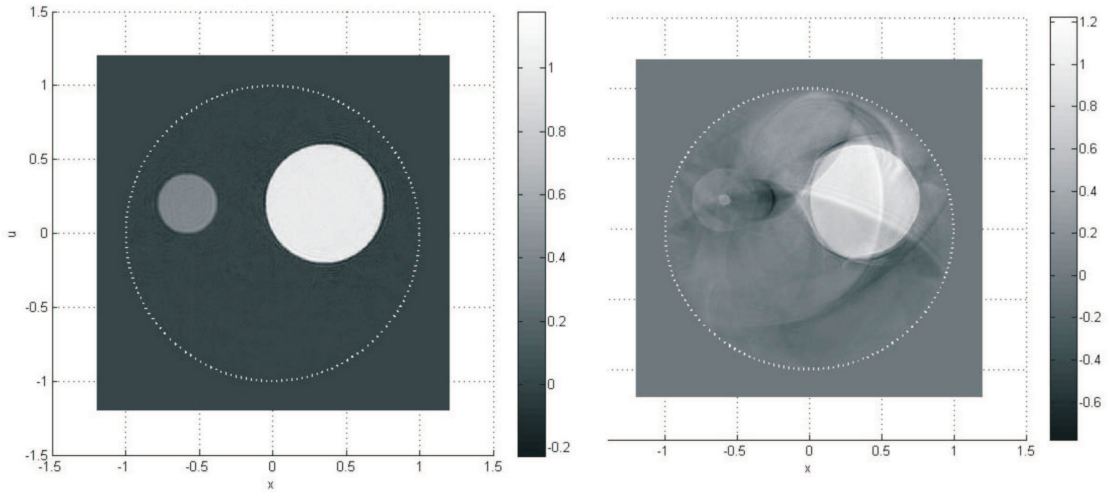

Figure 18. The reconstruction with the correct speed map (left) and with the average speed (right). One observes both location shifts and amplitude deterioration of the reconstruction with the average speed.

reconstruction. It would be extremely valuable, though, to be able to recover the speed map from the TAT data without any additional measurements. A numerical simultaneous reconstruction of the speed and the image was successfully attempted on examples in [68]. It is still an open question, however, to what extent the TAT data determines the sound speed. Below, we provide some preliminary discussion. It is planned to address this issue in more detail elsewhere.

A natural approach to the problem of recovery of the sound speed is the following. Consider the linear operator $L_{c(x)}$ that, given a sound speed $c(x)$, transforms the initial function $f(x)$ into the boundary TAT data $g(y,t)$ (see (1)). Then we would like to recover from the equation $L_{c(x)}f = g$ with a given g both the sound speed c and the image f. How can this be possible? A simple-minded objection is: given whatever c, one can solve this equation and find a solution f, and thus the equation does not carry any information about c. This argument, however, is correct only if the operators L_c are invertible, or "almost" invertible (in terms of the range of the operator being equal to almost the whole space of functions g). However, it is common in tomography that the range of the relevant operator (e.g., Radon or X-ray transforms, as well as our operator L_c) is very small, namely, of infinite co-dimension in natural spaces of functions g [42, 43]. Suppose that a range description for this transform is known (in appropriate spaces). A change of the sound speed leads to a "rotation" of the range. If the ranges rotate so much that their intersections for different sound speeds are only at the zero function, then given the data g, one could find out to the range of which operator $L_{c(x)}$ it belongs and thus determine $c(x)$. This would allow one to recover the sound speed, and then, using any of the methods described above, to reconstruct the image f. One can notice the similarity with the SPECT (single photon emission tomography), where

one faces the still not satisfactory resolved problem of the simultaneous recovery of the unknown attenuation coefficient (kind of an analog of the speed in TAT) and of the unknown source intensity distribution function [26, 42, 43, 56].

This approach requires knowledge of the range conditions, which are discussed in the next sub-section. Before doing this, though, we would like to mention that, as in SPECT, there might be some non-uniqueness of the speed recovery examples. The hope is, though, that this is not a general position situation in the space of sound speeds.

5.1. Range conditions

Range conditions for the case of a constant sound speed are well understood by now [2–4, 18, 34]. They contain two types of restrictions on the TAT data g: one concerns the smoothness and support of g and another involves orthogonality of g to certain functions.

We provide here without a proof an analog of (a part of) these results for the case of a variable sound speed $c(x)$, which is smooth, stabilizes to a constant $c > 0$ at large distances (and thus the support of $c(x) - c$ is compact), and satisfies the non-trapping condition (see Definition 2). The conditions described in the next theorem are necessary for a function g to belong to the range of $L_{c(x)}$, while we cannot claim the sufficiency of these conditions, as it was done for the constant speed case in the papers cited above. In fact, sufficiency would require some additional constrains.

As before, we denote by B the domain bounded by the observation surface S. Consider in the Hilbert space $L^2(c^{-2}(x), B)$ the operator $A := -c^2(x)\Delta$ with zero Dirichlet boundary conditions on S and the natural domain $H^2(B) \bigcap H_0^1(B)$. It is a positive self-adjoint operator. The following result is analogous to the ones of [3]:

Theorem 4. *Let $\{\lambda_k^2\}_{k=1}^{\infty}$ be the spectrum of A and ψ_k be the corresponding basis of orthonormal eigenfunctions in $L^2(c^{-2}(x), B)$. If $u(x,t)$ solves the problem*

$$\begin{cases} u_{tt}(x,t) - c^2(x)\Delta u(x,t) = 0, \text{ for all } x \in \mathbb{R}^n, t > 0 \\ u(x,0) = f(x) \in C_0^\infty(\mathbb{R}^n), \quad u_t(x,0) = 0, \\ u|_{S\times\mathbb{R}_+} = g, \end{cases}$$

then the function $g(x,t)$ on $S \times \mathbb{R}_+$ satisfies for any k the condition

$$\int_0^\infty \left(\int_S g(x,t) \frac{\partial \psi_k}{\partial \nu} \right) \cos(\lambda_k t) dt = 0, \tag{8}$$

where ν is the exterior unit normal vector to S.

The proof of this result is very similar to the one given in [3] for the constant speed case.

These conditions are not sufficient for g to be in the range of L_c, in particular since in the constant speed case there are additional conditions on the support of g that stem from the finite speed of propagation and Huygens' principle [3]. Thus, the theorem

above represents only the orthogonality type range conditions, while omitting support conditions.

In the next two sub-sections we will try to employ both the support and the orthogonality conditions to get some initial (and not conclusive yet) results on the uniqueness of the speed recovery.

5.2. Support range conditions and uniqueness of a constant speed

We first look at the simplest question: knowing in advance that the sound speed is constant, can one recover it from the TAT data? This question can be answered positively in odd dimensions $n > 1$, where the support conditions (due to Huygens' principle) alone are sufficient.

We will assume that the initial value $f(x)$ (the image to reconstruct) is compactly supported in the open ball $B = \{x||x| < 1\} \subset \mathbb{R}^n$, whose boundary $S = \{x||x| = 1\}$ is the observation surface. In other words, we assume that the support of $f(x)$ does not reach S. In this case, the finiteness of the speed of propagation shows that the boundary data $g(y,t)$ is equal to zero for small t. Let us thus define the first time $t_0 > 0$ when the signal reaches the boundary as follows:

$$t_0 = \inf\{t > 0| \text{ there exists } y \in S \text{ such that } g(y,t) \neq 0\}. \tag{9}$$

Since the speed of sound is constant and the dimension is odd, the Huygens' principle holds. Thus, the data g will vanish for large values of time t. We can define the last time $T_0 > 0$ when a non-zero signal is detected:

$$T_0 = \sup\{t > 0| \text{ there exists } y \in S \text{ such that } g(y,t) \neq 0\}. \tag{10}$$

The following result resolves the question of recovering a constant sound speed:

Theorem 5. *Let, as above, the initial perturbation f be supported inside the open ball B and the numbers $t_0, T_0 > 0$ be defined as in (9)-(10). Then the sound speed c satisfies the equality*

$$c = \frac{2}{t_0 + T_0} \tag{11}$$

and thus is uniquely determined by the TAT data g.

Proof The pressure wave $p(x,t)$ solves the following wave equation problem in $\mathbb{R}^n$:

$$\begin{cases} p_{tt}(x,t) - c^2 \Delta p(x,t) = 0, \quad t > 0, \\ p(x,0) = f(x), \\ p_t(x,0) = 0. \end{cases}$$

Let us denote by R the spherical mean type operator that transforms a function $f(x)$ into the function

$$(Rf)(x,t) = \int\limits_{|x-y|=t} f(y) dA(y),$$

where $dA(y)$ is the surface area measure on the sphere $|x-y|=t$.

The standard Kirchhoff-Poisson solution formulas for the wave equation (see [10] or [14, p. 77]) imply the representation

$$p(x,t) = c_n \left[\left(\frac{\partial}{\partial t} \frac{1}{t} \right)^{\frac{n-1}{2}} Rf \right](x,ct), \quad x \in \mathbb{R}^n, \quad t>0 \tag{12}$$

with a constant $c_n > 0$, whose exact value is irrelevant here.

In particular, for $y \in S$ we get

$$g(y,t) = c_n \left[\left(\frac{\partial}{\partial t} \frac{1}{t} \right)^{\frac{n-1}{2}} Rf \right](y,ct) \tag{13}$$

$$= 2^{\frac{n-1}{2}} c_n t \left[\left(\frac{1}{2t} \frac{\partial}{\partial t} \right)^{\frac{n-1}{2}} \frac{1}{t} Rf \right](y,ct) \tag{14}$$

$$= 2^{\frac{n-1}{2}} c_n t \left[\left(\frac{\partial}{\partial (t^2)} \right)^{\frac{n-1}{2}} \frac{1}{t} Rf \right](y,ct), \quad y \in S, \quad t>0. \tag{15}$$

The assumptions of the theorem imply that t_0 is the largest value of t such that $g(y,t)=0$ for all $t<t_0$.

Lemma 6. *The equality $g(y,t)=0$ being satisfied for all $y \in S$ and $t<t_0$ is equivalent to the equality $(Rf)(y,ct)=0$ being satisfied for all these values.*

Indeed, due to the formula (13), if $(Rf)(y,ct)=0$ for all $y \in S$ and $t<t_0$, this implies $g(y,t)=0$ in the same region. Let us now prove the converse statement. We recall that the assumption of the support of f not reaching S implies that $Rf(y,t)$ vanishes for sufficiently small values of t. On the other hand, the last formula in (13) implies that

$$\left[\left(\frac{\partial}{\partial (t^2)} \right)^{\frac{n-1}{2}} \frac{1}{t} Rf \right](y,ct) = 0$$

for all $y \in S$ and $t<t_0$. These two facts and integration with respect to t^2 imply that $(Rf)(y,ct)=0$ for all $y \in S$ and $t<t_0$. This proves the lemma.

The same argument (with $Rf=0$ for small values of t being replaced by the Huygens' principle), implies the following statement:

Lemma 7. *The equality $g(y,t)=0$ being satisfied for all $y \in S$ and $t>T_0$ is equivalent to the equality $(Rf)(y,ct)=0$ being satisfied for all these values.*

The above lemmas lead to an alternative description of the numbers t_0 and T_0 in terms of the spherical mean transform of f rather than the TAT data g:

Corollary 8. *The following formulas hold true:*

$$\begin{aligned} t_0 &= \tfrac{1}{c} \sup\{t : Rf(x,s)=0, \text{ for all } x \in S, s \le t\}, \\ T_0 &= \tfrac{1}{c} \inf\{t : Rf(x,s)=0, \text{ for all } x \in S, s \ge t\}. \end{aligned} \tag{16}$$

We will now use relations (16) to evaluate c in terms of t_0, T_0.

Let us define two quantities related to the support of f:

$$\sigma_0 = \min\{|x-y| : \quad x \in supp(f), y \in S\},$$
$$\Sigma_0 = \max\{|x-y| : \quad x \in supp(f), y \in S\}.$$

The following lemma clearly finishes the proof of the theorem:

Lemma 9. *The numbers σ_0, Σ_0 satisfy the following properties:*

(i) $\sigma_0 + \Sigma_0 = 2$.

(ii)

$$\sigma_0 = \sup\{t : Rf(x,s) = 0, \ \textit{for all } x \in S, s \le t\},$$
$$\Sigma_0 = \inf\{t : Rf(x,s) = 0, \ \textit{for all } x \in S, s \ge t\}.$$

(iii) $\sigma_0 = ct_0, \Sigma_0 = cT_0$

Proof of the lemma. Let us introduce the radius of the smallest ball centered at the origin that encloses the support of f:

$$r_0 = \sup\{|x| \,| \quad f(x) \neq 0\} < 1.$$

Then it is clear that $\sigma_0 = 1 - r_0$ and $\Sigma_0 = 1 + r_0$. This implies the first statement of the lemma. The third statement follows from the second one and the formulas (16).

It remains to prove the second statement of the lemma. In its generality, it follows from the non-trivial local uniqueness theorem for the spherical transform [39, Theorem 4]. This theorem, in particular, requires the support of f to be strictly inside S, which is one of our assumptions. However, in TAT applications, the initial function f is non-negative. Knowing this additional information, the statement is very easy to prove. Indeed, the following inequalities are obvious:

$$\sigma_0 \le \sup\{t : Rf(x,s) = 0, \ \text{for all } x \in S, s \le t\}, \tag{17}$$
$$\Sigma_0 \ge \inf\{t : Rf(x,s) = 0, \ \text{for all } x \in S, s \ge t\}. \tag{18}$$

It remains to prove that the inequalities

$$\sigma_0 < \sup\{t : Rf(x,s) = 0, \ \text{for all } x \in S, s \le t\} \tag{19}$$

and

$$\Sigma_0 > \inf\{t : Rf(x,s) = 0, \ \text{for all } x \in S, s \ge t\} \tag{20}$$

are impossible. Let us show this for the first of these inequalities. According to the definition of σ_0, there is a point $x_0 \in supp(f)$ such that the distance from x_0 to S is equal to σ_0. Let y_0 be the closest point to x_0 on S. Then Fubini theorem implies that for an arbitrarily small $\epsilon > 0$ there is a number $\sigma_0 < s < \sigma_0 + \epsilon$ such that the sphere $\{x \,| \, |x - y_0| = s\}$ intersects the support of f over a set of a positive surface measure. Due to the positivity of f, this implies that $(Rf)(y_0, s) \neq 0$. This proves the impossibility of the inequality (19). Impossibility of (20) is proven analogously.

This finishes the proof of the lemma and thus of the theorem. ∎

5.3. Orthogonality range conditions and speed determination

While in the previous sub-section we used successfully the support conditions for handling constant speeds, here we will make some observations concerning usage of the orthogonality conditions provided in Theorem 4 for the variable speed determination.

The conclusion we reach here is that these conditions alone do not guarantee uniqueness even for constant speeds. However, they do lead to a (rather weak) local uniqueness result.

Lemma 10. *The orthogonality conditions (23) alone do not determine a constant speed c uniquely.*

The following example in $3D$ proves the non-uniqueness. Let f be a radial function supported inside the unit ball B and u solves the problem

$$\begin{cases} u_{tt}(x,t) - \triangle u(x,t) = 0, \forall x \in \mathbb{R}^n, t > 0, \\ u(x,0) = f(x), \quad u_t(x,0) = 0. \end{cases} \tag{21}$$

Let $g = u|_{S\times\mathbb{R}^+}$. Then the range description says

$$\int_0^\infty \int_S g(x,t)\phi_k(x)\cos(\lambda_k t)dt = 0, \tag{22}$$

when ϕ_k is any spherical harmonic of degree k, and λ_k is a zero of the spherical Bessel function $j_{k+(n-2)/2}$.

Since f is radial, so is g, and thus the conditions need to be checked on radial functions (i.e., for $k = 0$) only:

$$\int_0^\infty \int_S g(x,t)\cos(\lambda t)dt = 0 \tag{23}$$

for λ being a zero of $j_{(n-2)/2}$.

Let us choose $n = 3$, and thus $j_{(n-2)/2}(\lambda) = j_{1/2}(\lambda) = \frac{\sin(\lambda)}{\lambda}$. We then have $\lambda = l\pi$. Therefore, if λ is a zero of $j_{(n-2)/2}$ then so is $m\lambda$ for any natural m. Now one can see that g satisfies the range conditions for the speed $c_1 = mc$ as well, which provides the needed counterexample.

It is clear that the counterexample would not work for the coefficient m being close to 1. This observation will lead to a (weak) local uniqueness result presented in the next theorem. First of all, we assume again that the speed $c(x) > 0$ is smooth, stabilizes to a constant at infinity, and satisfies the non-trapping condition.

Theorem 11. *Let the dimension $n > 1$ be odd, B be a bounded domain in $\mathbb{R}^n$ with a smooth boundary S, and g be a non-zero function on $S \times \mathbb{R}^+$ such that the problem*

$$\begin{cases} u_{tt} - c^2(x)\Delta u = 0, \quad x \in \mathbb{R}^n, t > 0, \\ u(x,0) \in C_0^\infty(\mathbb{R}^n), \quad u_t(x,0) = 0 \end{cases} \tag{24}$$

has a solution u satisfying $u|_{S^2\times\mathbb{R}_+} = g$.

Then there exists $\varepsilon_0 > 0$ such that for all $0 < |\varepsilon| < \varepsilon_0$, the problem

$$\begin{cases} u_{tt} - (1+\varepsilon)^2 c^2(x)\Delta u = 0, \quad x \in \mathbb{R}^n, t > 0, \\ u(x,0) \in C_0^\infty(\mathbb{R}^n), \quad u_t(x,0) = 0 \\ u|_{\partial\Omega\times\mathbb{R}_+} = g \end{cases}$$

has no solution.

Proof. Let λ_k^2 be an eigenvalue of the operator $A = -c^2(x)\Delta$ in B with zero Dirichlet conditions on S and ψ_k be an associated eigenfunction. Consider

$$G(t) = \int\limits_S g(x,t)\frac{\partial\psi_k}{\partial\nu}(x).$$

Notice that since g is not identically equal to zero and due to completeness of functions ψ_k in $L^2(c^{-2}(x), B)$, we can pick a value of k for which G is not identically equal to zero. We also have

$$|G(t)| \le \|\frac{\partial\psi_k}{\partial\nu}\|_{L^2(S)}\|g(\cdot,t)\|_{L^2(S)} \le C\|\frac{\partial\psi_k}{\partial\nu}\|_{L^2(S)}\|u(\cdot,t)\|_{H^1(B)}.$$

Due to the non-trapping condition imposed on $c(x)$ and dimension being odd, $\|u(\cdot,t)\|_{H^1(B)}$ decays exponentially at infinity, and hence so does $G(t)$. We extend G to an even function with respect to t and consider

$$\hat{G}(\xi) = \int\limits_{-\infty}^{\infty}\left(\int\limits_S g(x,t)\frac{\partial\psi_k}{\partial\nu}(x)\right)e^{i\xi t}dt.$$

Due to the exponential decay of G, this function is analytic in the strip $|Im(z)| < \delta$ for small enough $\delta > 0$. Since G, and hence $\hat{G}$, is not identically equal to zero, zeros of $\hat{G}$ are isolated. Moreover, the range conditions imply that λ_k is a zero of $\hat{G}$. Hence, there exists $\varepsilon_0 > 0$ such that $(1+\varepsilon)\lambda_k$ is not a zero of $\hat{G}$ for any ε such that $0 < |\varepsilon| < \varepsilon_0$.

On the other hand, suppose $g = v|_{S\times\mathbb{R}^+}$ for some v solving the problem

$$\begin{cases} v_{tt}(x,t) - \rho^2 c^2(x)\Delta v(x,t) = 0, \quad x \in \mathbb{R}^n, t > 0, \\ v(x,0) \in C_0^\infty(\mathbb{R}^n), \quad v_t(x,0) = 0. \end{cases} \tag{25}$$

Applying the range conditions with $c(x)$ replaced by $\rho c(x)$, and hence the zero λ_k replaced by $\rho\lambda_k$, we see that then $\hat{G}(\rho\lambda_k) = 0$. On the other hand, since $\rho \in (1-\varepsilon_0, 1+\varepsilon_0)$, this cannot happen. This finishes the proof.

6. Conclusions

A comparison of three main approaches (filtered backprojection, eigenfunction expansions, and time reversal) to inversion in thermoacoustic tomography is conducted (purely algebraic methods are not discussed). Underlying assumptions and restrictions of each of them are described. It is shown that the time reversal is the least restrictive among all. In particular, it allows sources outside the observation surface,

variable sound speed, arbitrary geometry of the (closed) observation surface, and non-zero initial time derivative of the pressure. Time reversal allows also for a simple numerical implementation, using which all the above features are confirmed in numerical experiments.

The role of non-trapping conditions is explained. It is noticed, in particular, that the best case for the time reversal is $3D$ with a non-trapping sound speed. However, it is shown in numerical experiments that time reversal works well even under the worst of circumstances: $2D$ problems with a trapping speed.

In the case of trapping speed, a limited-view type effect is noticed and explained.

The problem of recovery the sound speed from TAT measurements is discussed. Initial results on uniqueness of speed determination are obtained.

Acknowledgments

This work was supported in part by the NSF grants DMS 0604778 and 0648786. The authors express their gratitude to the NSF for the support. They also thank W. Bangerth, P. Burgholzer, D. Finch, H. Grün, L. Kunyansky, F. Natterer, G. Paltauf, B. Popov, and L.-H. Wang for information. Thanks also go to the reviewers for the comments that have helped to improve the text.

[1] M. Agranovsky and P. Kuchment, Uniqueness of reconstruction and an inversion procedure for thermoacoustic and photoacoustic tomography, Inverse Problems **23** (2007) 2089-2102.

[2] M. Agranovsky, P. Kuchment, and L. Kunyansky, On reconstruction formulas and algorithms for the thermoacoustic and photoacoustic tomography, a Chapter to appear in [60].

[3] M. Agranovsky, P. Kuchment, and E. T. Quinto, Range descriptions for the spherical mean Radon transform, J. Funct. Anal **248** (2007), 344–386.

[4] G. Ambartsoumian and P. Kuchment, A range description for the planar circular Radon transform, SIAM J. Math. Anal. **38(2)** (2006), 681–692.

[5] G. Ambartsoumian and S. Patch, Thermoacoustic tomography - implementation of exact backprojection formulas, arXiv:math.NA/0510638.

[6] P. Burgholzer, C. Hofer, G. Paltauf, M. Haltmeier, and O. Scherzer, Thermoacoustic tomography with integrating area and line detectors. IEEE Transactions on Ultrasonics, Ferroelectrics, and Frequency Control **52(9)** (2005), 1577–1583.

[7] P. Burgholzer, C. Hofer, G. J. Matt, G. Paltauf, M. Haltmeier, and O. Scherzer, Thermoacoustic tomography using a fiber-based Fabry-Perot interferometer as an integrating line detector, Proc. SPIE **6086** (2006), 434–442.

[8] P. Burgholzer, G. J. Matt, M. Haltmeier, and G. Paltauf, Exact and approximative imaging methods for photoacoustic tomography using an arbitrary detection surface, Phys. Rev. E **75** (2007), 046706.

[9] N. Burq, Décroissance de l'énergie locale de l'équation des ondes pour le problème extérieur et absence de résonance au voisinage du réel, Acta Math. **180** (1998), no. 1, 1–29.

[10] R. Courant and D. Hilbert, *Methods of Mathematical Physics, Volume II Partial Differential Equations*, Interscience, New York, 1962.

[11] G. J. Diebold, T. Sun, M. I. Khan, Photoacoustic monopole radiation in one, two, and three dimensions, Phys. Rev. Lett. **67** (1991), no. 24, 3384–3387.

[12] Yu. V. Egorov and M. A. Shubin, *Linear Partial Differential Equations. Foundations of the Classical Theory*, in *Partial Differential Equations. I.*, Yu. V. Egorov and M. A. Shubin (Editors), Encyclopaedia of Mathematical Sciences, v. 30, Springer Verlag 1992, pp. 1–259.

[13] L. Ehrenpreis, *The Universality of the Radon Transform*, Oxford Univ. Press 2003.

[14] L. C. Evans, *Partial Differential Equations*, AMS, Providence, RI 1998.

[15] D. Finch, Sound and light show: mathematics and photoacoustic tomography, Lecture at the Workshop on Bioimaging, J. Radon Inst. for Comp. and Appl. Math., Linz, Austria, November 12-17, 2007.

[16] D. Finch, M. Haltmeier, and Rakesh, Inversion of spherical means and the wave equation in even dimensions, SIAM J. Appl. Math. **68** (2007), no. 2, 392–412.

[17] D. Finch, S. Patch, and Rakesh, Determining a function from its mean values over a family of spheres, SIAM J. Math. Anal. **35** (2004), no. 5, 1213–1240.

[18] D. Finch and Rakesh, The range of the spherical mean value operator for functions supported in a ball, Inverse Problems **22**(2006),923–938.

[19] D. Finch and Rakesh, The spherical mean value operator with centers on a sphere, Inverse Problems **23**(2007), No. 6, S37–S50.

[20] H. Grün, M. Haltmeier, G. Paltauf, and P. Burgholzer, Photoacoustic tomography using a fiber based Fabry-Perot interferometer as an integrating line detector and image reconstruction by model-based time reversal method, Proc. SPIE, 2007, 6631, 663107.

[21] H. Grün, C. Hofer, M. Haltmeier, G. Paltauf, and P. Burgholzer, Photoacoustic tomography using a fiber based Fabry-Perot interferometer as an integrating line detector and image reconstruction by model-based time reversal method, Proc. Int. Congress on Ultrasonics, 2007.

[22] P. Günther, *Huygens' Principle and Hyperbolic Equations*, Academic Press, Boston, MA, 1988.

[23] M. Haltmeier, G. Paltauf, P. Burgholzer, and O. Scherzer, Thermoacoustic Tomography with integrating line detectors, Proc. SPIE **5864** (2005), 586402-8.

[24] M. Haltmeier, P. Burgholzer, C. Hofer, G. Paltauf, R. Nuster, and O. Scherzer, Thermoacoustic

tomography using integrating line detectors, Ultrasonics Symposium **1** (2005), 166–169.
[25] M. Haltmeier and O. Scherzer, Thermoacoustic tomography and the circular radon transform: exact inversion formula, Math. Models and Methods in Appl. Sci., **17** (2007), 635–655.
[26] A. Hertle, The identification problem for the constantly attenuated Radon transform, Math. Z. **197** (1988), 13–19.
[27] L. Hörmander, *The Analysis of Linear Partial Differential Operators*, v.1-4, Springer-Verlag, New York 1983-1985.
[28] X. Jin, and L. V. Wang, Thermoacoustic tomography with correction for acoustic speed variations, Physics in Medicine and Biology **51** (2006), 6437–6448.
[29] X. Jin, and L. V. Wang, Thermoacoustic reconstruction in acoustically heterogeneous media with the aid of ultrasound tomography, a Chapter to appear in [60].
[30] R. A. Kruger, W. L. Kiser, D. R. Reinecke, and G. A. Kruger, Thermoacoustic computed tomography using a conventional linear transducer array, Med. Phys. **30 (5)** (2003), 856–860.
[31] R. A. Kruger, P. Liu, Y. R. Fang, and C. R. Appledorn, Photoacoustic ultrasound (PAUS)reconstruction tomography, Med. Phys. **22** (1995), 1605-1609.
[32] P. Kuchment, Generalized Transforms of Radon Type and Their Applications, in [47], pp. 67–91.
[33] P. Kuchment, K. Lancaster, and L. Mogilevskaya (M. Mogilevsky), On local tomography, Inverse Problems, **11** (1995), 571–589.
[34] P. Kuchment and L. Kunyansky, Mathematics of thermoacoustic and photoacoustic tomography, European J. Appl. Math. **19** (2008), 1-34.
[35] P. Kuchment and E. T. Quinto, Some problems of integral geometry arising in tomography, chapter XI in [13].
[36] L. Kunyansky, Explicit inversion formulae for the spherical mean Radon transform, Inverse Problems **23** (2007), pp. 373–383.
[37] L. Kunyansky, A series solution and a fast algorithm for the inversion of the spherical mean Radon transform, Inverse Problems **23**(2007), No. 6, S11–S20.
[38] P. D. Lax, R. S. Phillips, *Scattering theory*, 2nd edition, Pure and Applied Mathematics, 26. Academic Press, Inc., Boston, MA, 1989.
[39] A. K. Louis and E. T. Quinto, Local tomographic methods in Sonar, in *Surveys on solution methods for inverse problems*, pp. 147-154, Springer, Vienna, 2000.
[40] C. S. Morawetz, The decay of solutions of the exterior initial boundary value problem for the wave equation, Comm. Pure Appl. Math. **14** (1961), 561–568.
[41] C. S. Morawetz, Decay of solutions of the exterior problem for the wave equation. Comm. Pure Appl. Math., **28** (1975), 229-264.
[42] F. Natterer, *The mathematics of computerized tomography*, Wiley, New York, 1986.
[43] F. Natterer and F. Wübbeling, *Mathematical Methods in Image Reconstruction*, Monographs on Mathematical Modeling and Computation v. 5, SIAM, Philadelphia, PA 2001.
[44] C. J. Nolan and M. Cheney, Synthetic aperture inversion, Inverse Problems **18**(2002), 221–235.
[45] S. J. Norton, Reconstruction of a two-dimensional reflecting medium over a circular domain: exact solution, J. Acoust. Soc. Am. **67** (1980), 1266-1273.
[46] S. J. Norton and M. Linzer, Ultrasonic reflectivity imaging in three dimensions: exact inverse scattering solutions for plane, cylindrical, and spherical apertures, IEEE Transactions on Biomedical Engineering, **28** (1981), 200–202.
[47] G. Olafsson and E. T. Quinto (Editors), *The Radon Transform, Inverse Problems, and Tomography. American Mathematical Society Short Course January 3–4, 2005, Atlanta, Georgia*, Proc. Symp. Appl. Math., v. 63, AMS, RI 2006.
[48] A. A. Oraevsky and A. A. Karabutov, In *Handbook of Optical Biomedical Diagonstics*, edited by V. V. Tuchin, SPIE, Bellingham, WA, Ch. 10, 2002
[49] A. A. Oraevsky and A. A. Karabutov, Optoacoustic Tomography, Ch. 34 In *Biomedical Photonics Handbook*, edited by T. Vo-Dinh, CRC, Boca Raton, FL, Chap. 34, 2003, **34**-1 – **34**-34.
[50] V. P. Palamodov, *Reconstructive Integral Geometry*, Birkhäuser, Basel 2004.

[51] G. Paltauf, P. Burgholzer, , M. Haltmeier, and O. Scherzer, Thermoacoustic Tomography using optical Line detection, Proc. SPIE **5864** (2005), 7–14.

[52] G. Paltauf, R. Nuster, M. Haltmeier, and P. Burgholzer, Thermoacoustic Computed Tomography using a Mach-Zehnder interferometer as acoustic line detector, Appl. Opt. **46** (16) (2007),3352–8.

[53] S. K. Patch and O. Scherzer, Photo- and Thermo-Acoustic Imaging, Inverse Problems **23**(2007), No. 6, S1–S10.

[54] E. T. Quinto, Singularities of the X-ray transform and limited data tomography in $\mathbf{R}^2$ and $\mathbf{R}^3$, SIAM J. Math. Anal. 24(1993), 1215–1225.

[55] J. V. Ralston, Solutions of the wave equation with localized energy, Comm. Pure Appl. Math., **22** (1969), 807–823.

[56] D. Solmon, The identification problem for the exponential Radon transform, Math. Methods in the Applied Sciences, 18(1995), 687-695.

[57] A. C. Tam, Applications of photoacoustic sensing techniques, Rev. Mod. Phys. **58** (1986), no. 2, 381–431.

[58] B. Vainberg, The short-wave asymptotic behavior of the solutions of stationary problems, and the asymptotic behavior as $t \to \infty$ of the solutions of nonstationary problems, Uspehi Mat. Nauk **30** (1975), no. 2(182), 3–55 (Russian). English translation: Russian Math. Surveys **30** (1975), no. 2, 1–58.

[59] B. Vainberg, *Asymptotics methods in the Equations of Mathematical Physics*, Gordon and Breach 1989. (Translation of the Russian 1982 edition).

[60] L. H. Wang (Editor), *Photoacoustic imaging and spectroscopy*, CRC Press, to appear.

[61] L. V. Wang and H. Wu, *Biomedical Optics. Principles and Imaging*, Wiley-Interscience 2007.

[62] X. Wang, Y. Pang, G. Ku, X. Xie, G. Stoica, L. Wang, Noninvasive laser-induced photoacoustic tomography for structural and functional *in vivo* imaging of the brain, Nature Biotechnology, **21** (2003), no. 7, 803–806.

[63] M. Xu and L.-H. V. Wang, Universal back-projection algorithm for photoacoustic computed tomography, Phys. Rev. E **71** (2005), 016706.

[64] M. Xu and L.-H. V. Wang, Photoacoustic imaging in biomedicine. *Review of Scientific Instruments*, **77**(2006):041101-01 – 041101-22.

[65] Y. Xu and L.-H. V. Wang, Effects of acoustic heterogeneity in breast thermoacoustic tomography, IEEE Trans. Ultrasonics, ferroelectrics, Frequency Control **50** (2003), no. 9, 1134–1146.

[66] Y. Xu, L. Wang, G. Ambartsoumian, and P. Kuchment, Reconstructions in limited view thermoacoustic tomography, Medical Physics 31(4) April 2004, 724–733.

[67] Y. Xu, L. Wang, G. Ambartsoumian, and P. Kuchment, Limited view thermoacoustic tomography, a Chapter to appear in [60].

[68] J. Zhang and M. A. Anastasio, Reconstruction of speed-of-sound and electromagnetic absorption distributions in photoacoustic tomography, Proceedings of SPIE **6086** (2006), 608619.